Differential Gain-of-Function Activity of Three p53 Hotspot Mutants *In Vivo*

Shunbin Xiong[1], Dhruv Chachad[1,2], Yun Zhang[3], Jovanka Gencel-Augusto[1,2], Mario Sirito[1], Vinod Pant[1], Peirong Yang[1], Chang Sun[1,2], Gilda Chau[1], Yuan Qi[4], Xiaoping Su[4], Elizabeth M. Whitley[5], Adel K. El-Naggar[6], and Guillermina Lozano[1]

ABSTRACT

The majority of *TP53* missense mutations identified in cancer patients are in the DNA-binding domain and are characterized as either structural or contact mutations. These missense mutations exhibit inhibitory effects on wild-type p53 activity. More importantly, these mutations also demonstrate gain-of-function (GOF) activities characterized by increased metastasis, poor prognosis, and drug resistance. To better understand the activities by which *TP53* mutations, identified in Li–Fraumeni syndrome, contribute to tumorigenesis, we generated mice harboring a novel germline *Trp53R245W* allele (contact mutation) and compared them with existing models with *Trp53R172H* (structural mutation) and *Trp53R270H* (contact mutation) alleles. Thymocytes from heterozygous mice showed that all three hotspot mutations exhibited similar inhibitory effects on wild-type p53 transcription *in vivo*, and tumors from these mice had similar levels of loss of heterozygosity. However, the overall survival of $Trp53^{R245W/+}$ and $Trp53^{R270H/+}$ mice, but not $Trp53^{R172H/+}$ mice, was significantly shorter than that of $Trp53^{+/-}$ mice, providing strong evidence for p53-mutant–specific GOF contributions to tumor development. Furthermore, $Trp53^{R245W/+}$ and $Trp53^{R270H/+}$ mice had more osteosarcoma metastases than $Trp53^{R172H/+}$ mice, suggesting that these two contact mutants have stronger GOF in driving osteosarcoma metastasis. Transcriptomic analyses using RNA sequencing data from $Trp53^{R172H/+}$, $Trp53^{R245W/+}$, and $Trp53^{R270H/+}$ primary osteosarcomas in comparison with $Trp53^{+/-}$ indicated that GOF of the three mutants was mediated by distinct pathways. Thus, both the inhibitory effect of mutant over wild-type p53 and GOF activities of mutant p53 contributed to tumorigenesis *in vivo*. Targeting p53 mutant–specific pathways may be important for therapeutic outcomes in osteosarcoma.

Significance: p53 hotspot mutants inhibit wild-type p53 similarly but differ in their GOF activities, with stronger tumor-promoting activity in contact mutants and distinct protein partners of each mutant driving tumorigenesis and metastasis.

Introduction

The *TP53* gene encodes a tetrameric transcription factor, p53, that binds a specific DNA sequence and activates hundreds of genes, many in a tissue-specific manner (1). Under normal conditions, p53 activity is low due to inhibition by MDM2 and MDM4 proteins (2). Under DNA damage and other stress signals, p53 is posttranslationally modified and stabilized to activate a transcriptional repertoire that induces cell-cycle arrest, senescence, apoptosis, and metabolic changes to inhibit cell transformation (3, 4).

Given these growth-suppressive pathways, the *TP53* tumor suppressor is frequently mutated or deleted in most human cancers. For example, 96% of high-grade serous ovarian cancers (5) and 80% of basal-like breast cancers (6) have *TP53* alterations. Additionally, 60% to 80% of "classic" Li–Fraumeni syndrome (LFS) patients have TP53 germline mutations with high risk of developing cancer at an early age (7). Osteosarcoma is a major cancer in LFS patients, especially in children. It is a rare cancer for which treatment options are limited (8).

Remarkably, among the *TP53* mutations found in human cancers, missense mutations predominate (9), including several hotspot p53 mutations located in the DNA-binding domain defined as either contact (R273H, R248Q, and R248W) or structural (R175H, G245S, R249S, and R282H) mutations based on a defective protein structure (10, 11). These mutant p53 proteins exhibit a range of activities that include: loss of wild-type (WT) activity and an inhibitory effect (IE) that reduces WT p53 activity (12), and gain-of-function (GOF) activities (13). Mutant and WT p53 proteins form mixed tetramers to inhibit WT p53 activity, often in a context-dependent manner (12). In addition to inhibition of WT p53 activities by mutant p53, compelling evidence shows that mutant p53 proteins have novel GOF activities that contribute to tumorigenesis and metastasis. $Trp53^{R172H/+}$ and $Trp53^{R270H/+}$ mice (mimicking human LFS *TP53R175H* and *TP53R273H* mutations, respectively) develop tumors with increased metastasis as compared with $Trp53^{+/-}$ mice (14, 15). Numerous studies identified multiple mechanisms of GOF activities of mutant p53 that contribute to increased invasiveness and metastatic potential (13, 16). In general terms, p53-mutant proteins can interact with other cellular proteins (some of which are tissue-specific) disrupting their normal functions or usurping their

[1]Department of Genetics, The University of Texas MD Anderson Cancer Center, UT Health Graduate School of Biomedical Sciences, Houston, Texas. [2]Genetics and Epigenetics Graduate Program, The University of Texas MD Anderson Cancer Center, UT Health Graduate School of Biomedical Sciences, Houston, Texas. [3]Department of Pharmaceutical Sciences, College of Pharmacy and Health Sciences, Texas Southern University, Houston, Texas. [4]Department of Bioinformatics and Computational Biology, The University of Texas MD Anderson Cancer Center, Houston, Texas. [5]Department of Veterinary Medicine and Surgery, The University of Texas MD Anderson Cancer Center, Houston, Texas. [6]Department of Pathology, The University of Texas MD Anderson Cancer Center, Houston, Texas.

Note: Supplementary data for this article are available at Cancer Research Online (http://cancerres.aacrjournals.org/).

Corresponding Author: Guillermina Lozano, Department of Genetics Unit 1010, The University of Texas MD Anderson Cancer Center, 1515 Holcombe Boulevard, Houston, TX 77030. Phone: 713-834-6386; E-mail: gglozano@mdanderson.org

Cancer Res 2022;82:1926–36

doi: 10.1158/0008-5472.CAN-21-3376

transcriptional functions to alter the transcriptome. Although mutant p53 proteins drive tumor development by multiple mechanisms, these mechanisms are not necessarily mutually exclusive. In addition, these mechanisms are cancer type– and cell context–dependent (13, 17).

Unequal tumorigenic effects of *TP53* missense mutations in LFS patients have been noted (18). Knock-in mouse models that mimic patients with LFS have also been developed (19). *Trp53R172H* (a structural mutant) and *Trp53R270H* (a contact mutant) mice were generated with the *Trp53R270H* mouse model exhibiting a distinct spontaneous tumor spectrum from the *Trp53R172H* mouse, indicating that different missense mutations may drive tumorigenesis differently (15). Although a humanized *TP53R258W* knock-in (HUPKI) mouse was generated (20), a comparable *Trp53R248W* mouse model has not been developed to date. To better understand the mutant-specific phenotypes of mice mimicking the human *TP53R248W* mutation, and to explore the IE and GOF *in vivo*, a germline $Trp53^{R245W}$ allele was generated. The IE and GOF of p53R245W were compared with two previously published LFS mutations, p53R172H and p53R270H. All three showed comparable IE on WT p53 activities. Contact mutations p53R245W and p53R270H showed stronger GOF than the structural mutation p53R172H. In addition, osteosarcomas for all three alleles showed distinct GOF mechanisms drive tumorigenesis.

Materials and Methods

Mice and tumor analyses

Genotyping was performed by polymerase chain reaction (PCR) as previously described (21). *Zp3-cre* and $Trp53^{R270H/+}$ mice were purchased from The Jackson Laboratory. $Trp53^{R270H/+}$ mice (15) were backcrossed to C57BL/6J for three generations to obtain a background (>92% C57BL/6J) similar to $Trp53^{R172H/+}$ and $Trp53^{R245WH/+}$ mice. Mouse cohorts were monitored daily for tumorigenesis. Moribund mice were euthanized, and tissues were fixed in 10% v/v formalin and embedded in paraffin. Sections were stained with hematoxylin and eosin for pathologic analyses. All mouse experiments were approved by the Institutional Animal Care and Use Committee of MD Anderson Cancer Center and in compliance with the US Public Health Service Policy on Humane Care and Use of Laboratory Animals.

p53 and cleaved caspase-3 (CC3) IHC was performed as described previously with CM5 and CC3 (22) antibodies, respectively. The Vector DAB Substrate Kit (Vector Laboratories) was used for chromogenic detection. The percentage of p53-positive nuclei was determined using ImageJ software. To examine loss of heterozygosity (LOH) of *p53*, primers spanning the missense mutations were used to amplify tumor DNA samples by PCR; the PCR products were then sequenced. LOH was measured as loss of 80% of WT p53 peaks as previously described (21). The primers for detecting LOH in $Trp53^{R270H/+}$ tumors were the following: In7FW: CCAGCTTTCTTACTGCCTTGTGC; Ex8Rev: GCAGTTCAGGGCAAAGGACTTCC.

Cell culture, immunoprecipitation, Western blot analysis, and reverse transcription quantitative PCR

Male mice (age 4–8 weeks) or mouse embryonic fibroblasts (MEF) were irradiated at 2.5 or 6 Gy, and protein lysates and total RNA were prepared from the mouse tissues or MEFs 4 hours later. The protein lysates were prepared by homogenizing mouse tissues directly in SDS-PAGE loading buffer, followed by sonication for 1 to 2 minutes. Cell lines 0263 and H318 were generated previously (23), H222 was generated from $Trp53^{R172H/+}$, 14W and 55W from $Trp53^{R245W/+}$, 26R and 752R from $Trp53^{R270H/+}$ primary osteosarcomas. The cell lysates were prepared in NP-40 buffer and immunoprecipitated using Glial fibrillary acidic protein (Dako Z033401) or p53 antibody (Leica; cat. #NCL-L-p53-CM5p). Antibodies used for western blots were: Cdkn1a (p21; 1:1,000) (Cell Signaling Technology; cat. #2947, RRID: AB_823586); vinculin (1:5,000; Sigma-Aldrich, V9264); Egr1(1:1,000; Thermo Fisher, MA5-15008); signal transducer and activator of transcription 3 (Stat3; 1:1,000; Thermo Fisher, MA5-15712). Total RNA was prepared from cells or tissues by TRIzol reagent (Invitrogen 15596-026) and then treated with DNase I (Roche). Reverse transcription quantitative PCRs (RT-qPCR) of p53 downstream target genes *Eda2r, p21, Mdm2, Bbc3* (Puma), and *Pmaip1*(*Noxa)* were performed as reported previously (1, 24). Data were normalized to *Gapdh* or *Rplp0*.

Transcriptomic analyses of murine osteosarcomas and siRNA-treated $Trp53^{R245W/+}$ tumor cell line

The primary osteosarcomas from $Trp53^{+/-}$, $Trp53^{R172H/+}$, $Trp53^{R245W/+}$, and $Trp53^{R270H/+}$ mice were collected at the time of necropsy, snap-frozen using liquid nitrogen, and stored at −80°C. The tumors were crushed to powder using a mortar and pestle, and approximately 100 mg of powder was used to isolate RNA using a Direct-zol RNA Microprep Kit (Zymo Research, R2062). Osteosarcoma cell line 14W was transfected with either p53siRNAs (Si-1 and Si-2) or control siRNA (MilliporeSigma, SASI_Mm02_00310137, SASI_Mm02_00310139 and SiC001), total RNAs were isolated 48 hours after the transfection using RNeasy Mini Kit (Qiagen 74004). RNA was submitted to the Advanced Technology Genomics Core at The University of Texas MD Anderson Cancer Center for bulk RNA-sequencing as described (25). Read mapping was performed using STAR RRID: SCR_004463 and GRCm38 (MM10) was used as the reference genome. The program FastQC, RRID:SCR_014583 (v. 0.11.5) was used to check for quality of FASTQ reads. Annotation of genes was carried out using the GENCODE, RRID:SCR_014966 (v. 3.6.0) and the Bioconductor, RRID:SCR_006442 package was used for analysis.

Differentially expressed genes (DEG) were identified using DESeq2, RRID:SCR_000154. The read count was first prefiltered to keep genes that had 5 or more reads in 3 or more samples. DESeq2 modeled the counts using a negative binomial distribution, followed by the Wald test. The final *P* value was adjusted using the Benjamini and Hochberg method. Significant DEGs were selected based on the criteria of adjusted *P* value < 0.05 ($P_{adj} < 0.05$) when the mutant *Trp53* cohorts were compared with the heterozygous *Trp53* cohort. To identify potential mutant p53-associated transcription factors that lie upstream of differentially upregulated genes, data from JASPAR, TRANSFAC, ENCODE, ChEA, and Targetscan databases were used by considering the overlap between Enrichr, oPOSSUM, and Ingenuity Pathway Analysis (Ingenuity Pathway Analysis, RRID:SCR_008653, Invitrogen). This approach allowed us to avoid experimental bias and discrepancies introduced due to z-score and *P* value cutoffs in different algorithms. IPA was also used to identify dysregulated pathways in the mutant *Trp53* cohorts using DEGs.

Statistical analysis

Student *t* tests and Kaplan–Meier survival analyses were performed with PRISM, RRID:SCR_005375, version 9). *P* values of < 0.05 were considered to be statistically significant.

Data availability statement

RNA-seq data sets generated in this study have been deposited in Gene-Expression Omnibus under accession number GSE198802.

Results

Generation and characterization of *p53R245W* mice

To generate a knock-in mouse model with the p53R245W mutation (representing the hotspot p53R248W mutation in humans), we took advantage of the conditional $Trp53^{wm\text{-}R245W}$ allele previously characterized (21). $Trp53^{wm\text{-}R245W}$ expresses WT p53 but converts to p53R245W-mutant expression upon Cre-mediated deletion of WT sequences. $Trp53^{wm\text{-}R245W}$ mice were crossed with *Zp3-Cre* mice, and subsequently to C57BL/6J mice to generate germline $Trp53^{R245W/+}$ mice (Supplementary Fig. S1A). After removal of the *Cre* transgene, interbreeding of $Trp53^{R245W/+}$ mice produced a normal Mendelian ratio of expected genotypes, indicating no lethal consequences of $Trp53^{R245W/R245W}$ homozygosity (Supplementary Table S1).

To test whether the *Trp53R245W* allele is a loss-of-function allele *in vivo*, we examined its ability to rescue the *Mdm2-null* early lethal phenotype as does *p53* deletion but not *p53* heterozygosity (26, 27). In several crosses, the expected number of $Mdm2^{-/-}Trp53^{R245W/R245W}$ mice were observed at weaning, indicating that homozygosity of the *Trp53R245W* allele completely rescues the embryonic lethality of $Mdm2^{-/-}$ mice (Supplementary Table S2), demonstrating little or no WT activity of the p53R245W protein. To examine the transcriptional activity of p53R245W after DNA damage, the relative RNA levels of canonical p53 downstream targets cyclin-dependent kinase inhibitor 1A (*Cdkn1a*, or *p21*) and *Bbc3 (Puma)* were examined by qRT-PCR in the spleens of mice treated with ionizing radiation (IR). $Trp53^{R245W/R245W}$ mice showed no transcriptional activity after 6 Gy IR exposure (Supplementary Fig. S1B), as would be expected from an allele that lost WT p53 activity. p21 protein was also not induced in $Trp53^{R245W/R245W}$ mouse spleens or in MEFs after 6 Gy IR (Supplementary Fig. S1C and S1D). These results indicated that p53R245W has little if any WT p53 activity.

Similar IE from different p53 mutations *in vivo*

To investigate whether p53R172H, p53R245W, and p53R270H proteins exert IE over WT p53 *in vivo*, heterozygous $Trp53^{R172H/+}$, $Trp53^{R245W/+}$, and $Trp53^{R270H/+}$ mice (collectively $Trp53^{Mut/+}$) were irradiated with 2.5 Gy, a dose that distinguishes small differences in WT p53 activity (28). The relative mRNA levels of p53 downstream target genes *Eda2r*, *Cdkn1a* (*p21*), *Bbc3 (Puma)*, *Bax*, and *Ccng1* in thymuses were measured by RT-qPCR. In comparison with the $Trp53^{+/-}$ mice, all $Trp53^{R172H/+}$, $Trp53^{R245W/+}$, and $Trp53^{R270H/+}$ mice showed comparable decreased activation of these downstream target genes, which were not statistically different from each other (**Fig. 1A**). No activation of target genes was observed in $Trp53^{-/-}$ mice after irradiation, demonstrating that the assay was specific for p53 activity (**Fig. 1A**). Moreover, the activation of all genes among

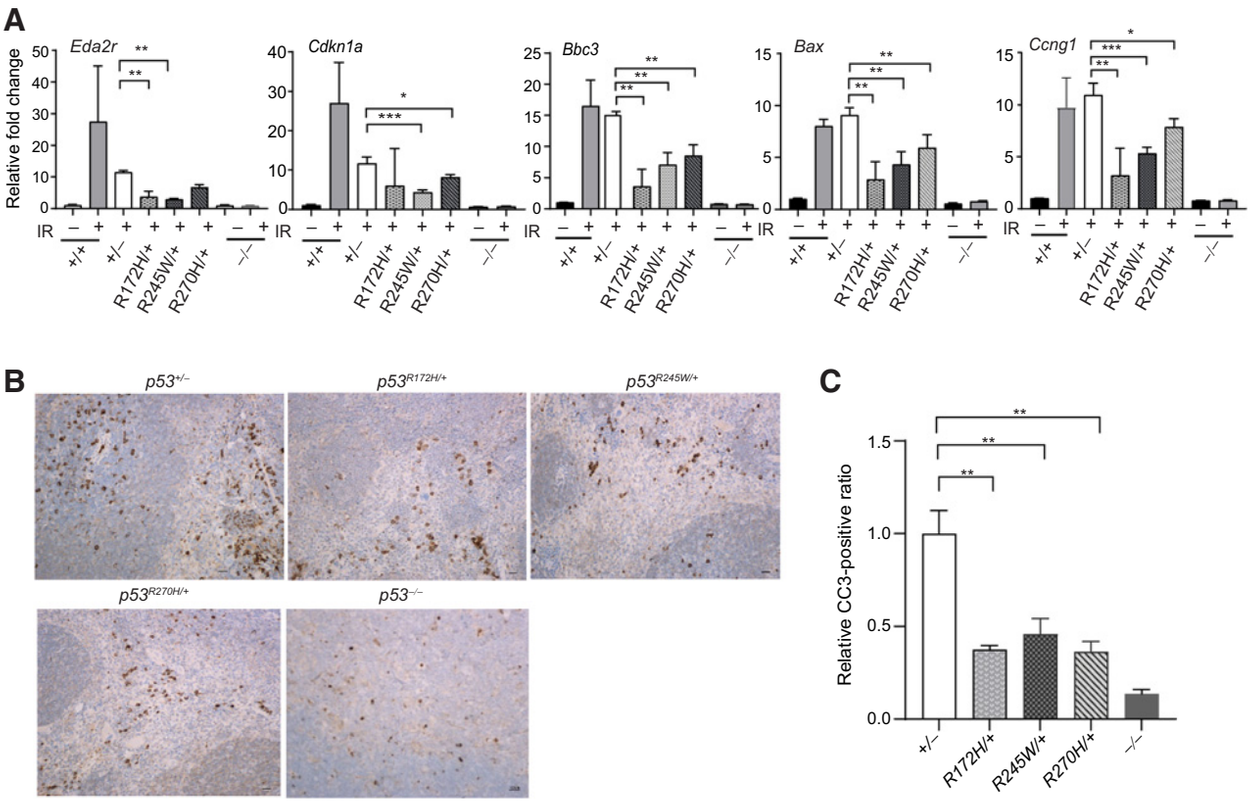

Figure 1.

Similar IE among p53 mutations *in vivo*. **A,** RNA levels of p53 downstream target genes *Eda2r*, *Cdkn1a* (*p21*), *Bbc3* (*Puma*), *Bax*, and *Ccng1* were determined by RT-qPCR 4 hours after 2.5 Gy irradiation in *WT* (+/+; $N = 4$ for both non-IR and IR treatment), $Trp53^{+/-}$ (+/−; $N = 3$), $Trp53^{R172H/+}$ (*R172H/+*; $N = 5$), $Trp53^{R245W/+}$ (*R245W/+*; $N = 4$), $Trp53^{R270H/+}$ (*R270H/+*; $N = 4$), and $Trp53^{-/-}$ (−/−; $N = 3$ for non-IR and $N = 5$ for IR) mouse thymuses. **B,** IHC staining of CC3 was performed on thymus tissues from mice with the indicated genotypes. Scale bar, 100 μm. **C,** CC3-stained cells were quantified in five random fields. *, $P < 0.05$; **, $P < 0.01$; ***, $P < 0.001$ by the *t* test.

heterozygous mice was higher than in $Trp53^{-/-}$ mice, indicating partial inhibition of WT p53 activity by mutant p53. To explore the IE on p53-induced apoptosis, we performed IHC staining with CC3 antibodies on IR-treated thymuses. $Trp53^{R172H/+}$, $Trp53^{R245W/+}$, and $Trp53^{R270H/+}$ mice showed less CC3 staining than $Trp53^{+/-}$ mice but more than $Trp53^{-/-}$ mice again indicative of a similar IE of mutant p53 on WT p53 function (**Fig. 1B** and **C**). Thus, two different assays indicate that mutant p53 exerts an IE on WT p53.

$Trp53^{neo/-}$ mice express approximately 7% of the WT p53 protein (due to insertion of the *Neo* gene into the WT *p53* locus within intron 4 near the internal promoter), yet show delayed tumorigenesis as compared with $Trp53^{-/-}$ mice, indicating that even a low level of p53 is tumor suppressive (22). Additionally, $Trp53^{neo/R172H}$ mice have significantly shorter survival than $Trp53^{neo/-}$ mice, indicating an IE of p53R172H on WT p53 during tumor development (22). To compare the IE among all three p53 mutants in this model *in vivo*, we generated $Trp53^{neo/R172H}$, $Trp53^{neo/R245W}$, and $Trp53^{neo/R270H}$ mice (collectively $Trp53^{neo/Mut}$) and compared with $Trp53^{neo/-}$ mice. To measure transcriptional activity, mice were irradiated at 6 Gy at about 1 month of age, and p53 downstream target genes in the thymuses were examined by RT-qPCR. The 6 Gy dose was required because of the low p53 levels produced by the $Trp53^{neo}$ allele. The expression of *Cdkn1a* (*p21*), *Bax*, and *Bbc3* (*Puma*) was clearly less activated (if at all) in $Trp53^{neo/Mut}$ mice than in $Trp53^{neo/-}$ mice indicative of an IE of mutant on WT p53 (**Fig. 2A**). To further compare the effects of mutant p53 on tumor development, mice were monitored for spontaneous tumorigenesis. The major tumor types that developed in these mice were lymphomas (about 60%). The median overall survival of $Trp53^{neo/R172H}$, $Trp53^{neo/R245W}$, $Trp53^{neo/R270H}$ mice was similar (136, 141, 153 days, respectively) to $Trp53^{-/-}$ mice (160 days) and had no statistically significant difference. However, all three cohorts exhibited significantly shorter survival than the $Trp53^{neo/-}$ mice (218 days; **Fig. 2B**), indicating all three p53 hotspot mutations had a similar IE on WT p53 activity during spontaneous tumorigenesis.

Tumors frequently undergo LOH in the context of WT *Trp53* alleles. Even though this $Trp53^{neo}$ allele is a hypomorph, we evaluated if there were any differences in $Trp53^{neo}$ allele retention between the $Trp53^{neo/Mut}$ and $Trp53^{neo/-}$ tumors. We assayed for its presence in 30

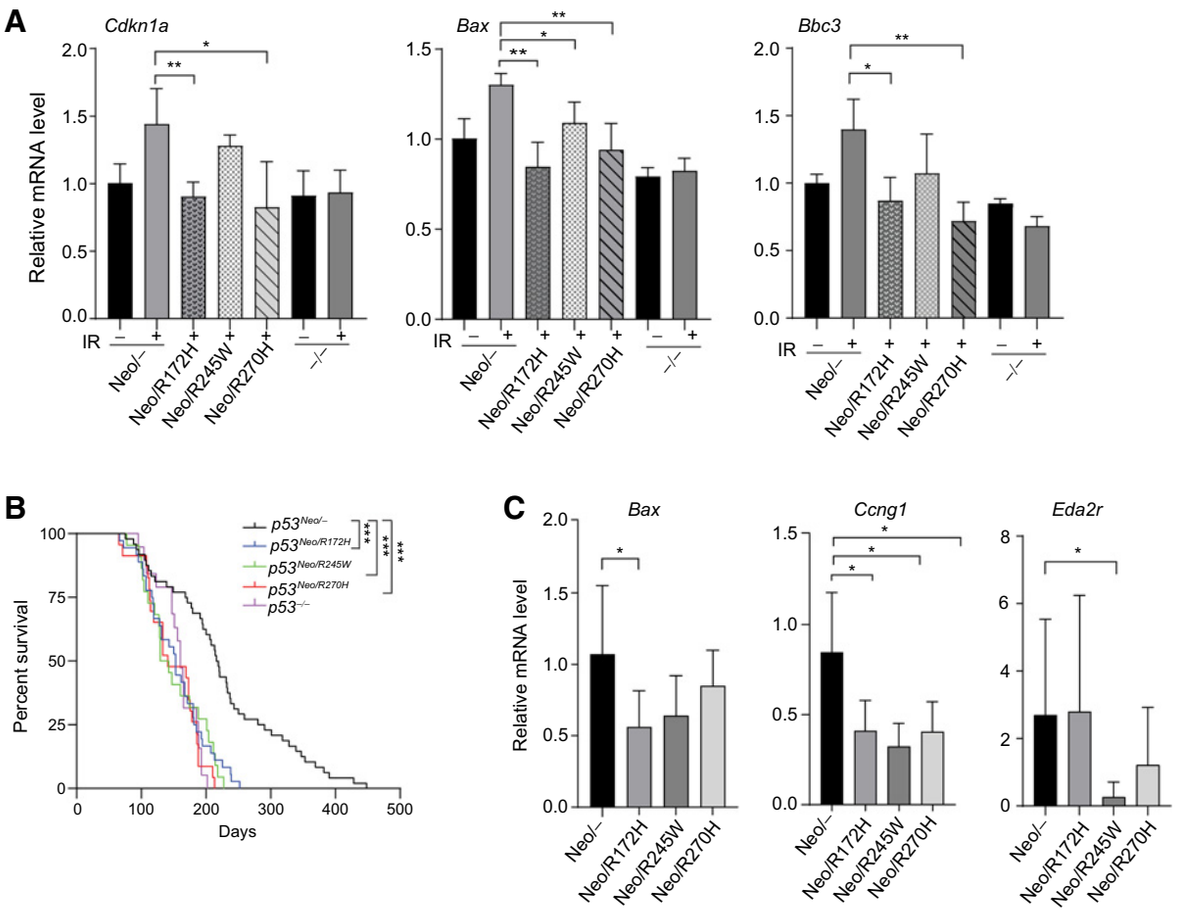

Figure 2.

IE of mutant p53 *in vivo*. **A,** IE of mutant p53 by IR treatment in $Trp53^{neo/-}$ and $Trp53^{neo/mut}$ mice. Relative RNA levels of *Cdkn1a* (*p21*), *Bax*, and *Bbc3* (*Puma*) were determined by RT-qPCR in thymuses of 1-month-old $Trp53^{neo/-}$ (Neo/−), $Trp53^{neo/R172H}$ (Neo/R172H), $Trp53^{neo/R245W}$ (Neo/R245W), $Trp53^{neo/R270H}$ (Neo/R270H), and $Trp53^{-/-}$ (−/−) mice, 4 hours after 6 Gy IR treatment. At least three mice were used for each genotype. **B,** Kaplan–Meier survival curves of $Trp53^{neo/-}$ ($N = 48$), $Trp53^{neo/R172H}$($N = 36$), $Trp53^{neo/R245W}$ ($N = 22$), $Trp53^{neo/R270H}$ ($N = 23$), and $Trp53^{-/-}$ ($N = 19$) mice. **C,** Expression of p53 target genes in $Trp53^{neo/Mut}$ tumors compared with $Trp53^{neo/-}$ tumors was determined by RT-qPCR. *, $P < 0.05$; **, $P < 0.01$; ***, $P < 0.001$ by the *t* test.

tumors (6 from $Trp53^{neo/-}$ mice, 10 from $Trp53^{neo/R172H}$ mice, 7 from $Trp53^{neo/R245W}$ mice, and 7 from $Trp53^{neo/R270H}$ mice). All tumors, except 1 $Trp53^{neo/R245W}$ tumor, retained the $Trp53^{neo}$ allele as determined by Sanger sequencing. Because tumors retained a WT p53 allele (albeit a weak one), we were able to examine whether the WT p53 transcriptional program was repressed by mutant p53 in tumors at endpoint. The expression levels of p53 downstream target genes *Bax, Ccng1*, and *Eda2r* were expressed significantly lower in $Trp53^{neo/R172H}$, $Trp53^{neo/R245W}$, and $Trp53^{neo/R270H}$ tumors in comparison with $Trp53^{neo/-}$ tumors as measured by RT-qPCR

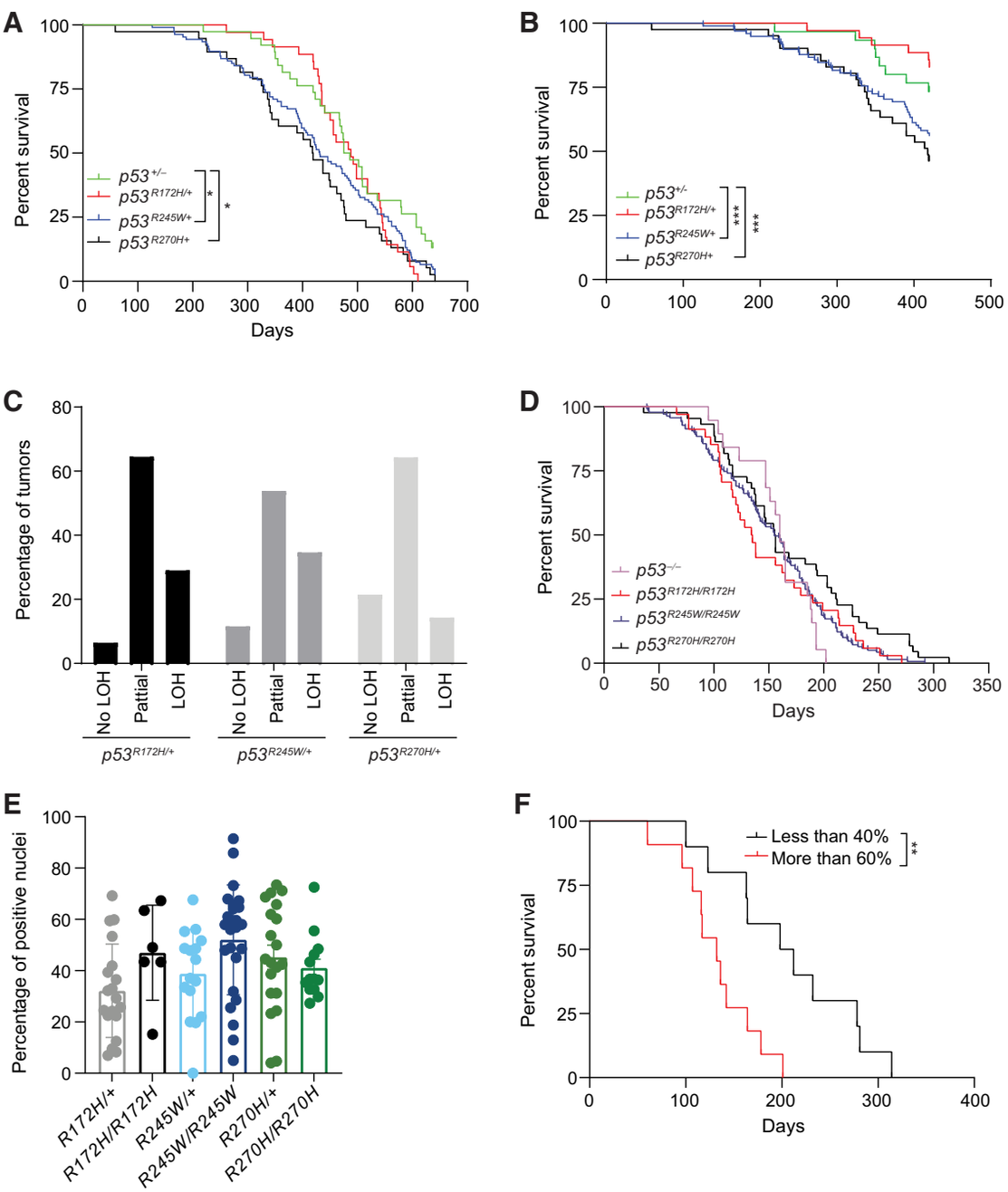

Figure 3.

Distinct tumor phenotypes among mutant p53 mice. **A** and **B,** Kaplan–Meier survival curves of $Trp53^{+/-}$ ($N = 33$), $Trp53^{R172H/+}$ ($N = 35$), $Trp53^{R245W/+}$ ($N = 105$), and $Trp53^{R270H/+}$ ($N = 38$) mice at 22 months (**A**) and 14 months (**B**). **C,** LOH analysis in $Trp53^{R172H/+}$ ($N = 31$), $Trp53^{R245W/+}$ ($N = 26$), and $Trp53^{R270H/+}$ ($N = 14$) tumors. **D,** Kaplan–Meier survival curves of $Trp53^{-/-}$ ($N = 19$), $Trp53^{R172H/R172H}$ ($N = 34$), $Trp53^{R245W/R245W}$ ($N = 139$), and $Trp53^{R270H/R270H}$ ($N = 44$) mice. **E,** p53 levels were detected by IHC staining in $Trp53^{R172H/+}$ ($N = 19$), $Trp53^{R172H/R172H}$ ($N = 6$), $Trp53^{R245W/+}$ ($N = 16$), $Trp53^{R245W/R245W}$ ($N = 25$), $Trp53^{R270H/+}$ ($N = 20$), and $Trp53^{R270H/R270H}$ ($N = 13$) tumors. Positively stained nuclei were counted by ImageJ software. **F,** Kaplan–Meier survival curves of homozygous $Trp53^{R245W/R245W}$ and $Trp53^{R270H/R270H}$ mice with 0%–40% and 60%–100% positive p53 nuclei by IHC staining. *, $P < 0.05$; **, $P < 0.01$; ***, $P < 0.001$ by the *t* test.

(**Fig. 2C**), supporting IE activity of all three p53-mutant alleles *in vivo*.

Tumorigenesis among different mutant *p53* alleles

To compare the roles of p53R172H, p53R245W, and p53R270H-mutants versus *Trp53* loss in spontaneous tumorigenesis with a genotype consistent with LFS patients, a cohort of $Trp53^{R172H/+}$ ($N = 35$), $Trp53^{R245W/+}$ ($N = 105$), $Trp53^{R270H/+}$ ($N = 38$), and $Trp53^{+/-}$ ($N = 33$) mice with a similar genetic background were generated. Consistent with previous studies (14, 15), the overall survival of $Trp53^{R172H/+}$ mice did not differ significantly from that of $Trp53^{+/-}$ mice (median survival at 488 and 486 days, respectively). However, the overall survival of $Trp53^{R245W/+}$ and $Trp53^{R270H/+}$ mice (median survival at 431 and 419 days, respectively) were significantly shorter than that of the $Trp53^{+/-}$ mice ($P = 0.036$ and 0.012, respectively) but not that of $Trp53^{R172H/+}$ mice when the cohorts were monitored for up to 22 months (**Fig. 3A**). Additionally, when surveyed at 14 months of age, the differences in overall survival between both $Trp53^{R245W/+}$ and $Trp53^{R270H/+}$ mice, as compared with $Trp53^{R172H/+}$ mice were significant ($P = 0.005$ and 0.0007, respectively; **Fig. 3B**). These data suggested that $Trp53^{R245W/+}$ and $Trp53^{R270H/+}$ mice were more prone to tumor development than $Trp53^{R172H/+}$ mice, indicating p53R245W and p53R270H-mutants were more potent than the p53R172H mutant in driving spontaneous tumorigenesis *in vivo*. The major cancer these mice developed were sarcomas, which varied from 37% to 60% (**Table 1**). Osteosarcomas, in particular, occurred in 17% to 33% of mice and were more prevalent in female mice (see below). Lymphomas were the second most common tumor observed (20%–30%). More carcinomas were observed in $Trp53^{R172H/+}$ (15%), $Trp53^{R245W/+}$ (27%), and $Trp53^{R270H/+}$ (23%) mice as compared with $Trp53^{+/-}$ (8%) mice. In particular, lung adenocarcinomas were found in $Trp53^{R172H/+}$ (3%), $Trp53^{R245W/+}$ (11%), and $Trp53^{R270H/+}$ (17%) mice but not in $Trp53^{+/-}$ mice, indicating mutation-specific tumor types compared with *p53* loss. Importantly, metastases of sarcomas and carcinomas were observed only in $Trp53^{Mut/+}$ and not in $Trp53^{+/-}$ mice indicative of GOF activities for mutant p53 proteins.

To investigate whether LOH of the WT *Trp53* allele contributes to differences in tumorigenesis among these $Trp53^{Mut/+}$ cohorts, LOH analyses were performed in $Trp53^{R172H/+}$ ($N = 31$), $Trp53^{R245W/+}$ ($N = 26$), and $Trp53^{R270H/+}$ ($N = 14$) tumors, including lymphomas, carcinomas, and sarcomas (**Table 1**). For all three cohorts, the WT *Trp53* allele was retained in 65% to 86% of tumors while completely lost in 14% to 35%, and the percentages of zero, partial, or complete LOH were statistically similar among the three cohorts (**Fig. 3C**). Thus, it is unlikely that LOH of WT *p53* in tumors contributes to the difference in overall survival among $Trp53^{Mut/+}$ mice. The shorter overall survival of $Trp53^{R245W/+}$ and $Trp53^{R270H/+}$ mice suggested that contact mutations p53R245W and p53R270H are more tumorigenic than *p53* loss in a heterozygous background.

Additionally, homozygous $Trp53^{R172H/R172H}$, $Trp53^{R245W/R245W}$, and $Trp53^{R270H/R270H}$ mice were monitored for tumorigenesis as well, and the median overall survival (134.5, 154, and 155.5 days, respectively) was similar to $Trp53^{-/-}$ (160 days; **Fig. 3D**). Although similar percentages of lymphoma were observed among all three homozygous cohorts, 4 of 89 $Trp53^{R245W/R245W}$ mice and 2 of 29 $Trp53^{R270H/R2700H}$

Table 1. Tumor spectrum in $Trp53^{R172H/+}$, $Trp53^{R245W/+}$, and $Trp53^{R270H/+}$ mice.

	Genotype			
Tumor type	***Trp53*$^{+/-}$ (*N* = 25)**	***Trp53*$^{R172H/+}$ (*N* = 34)**	***Trp53*$^{R245W/+}$ (*N* = 46)**	***Trp53*$^{R270H/+}$ (*N* = 24)**
Lymphoma	6 (24%)	10 (29%)	19 (30%)	6 (20%)
Sarcoma	15 (60%)	15 (44%)	23 (37%)	16 (53%)
Osteosarcoma	7 (28%)	8 (24%)[a]	11 (17%)[b]	10 (33%)[c]
Angiosarcoma	1 (4%)	1 (3%)	6 (10%)	1 (3%)
Spindle cell sarcoma	3 (12%)	3 (9%)	3 (5%)	1 (3%)
Sarcoma (synovia)				1 (3%)
Sarcoma, NOS	4 (16%)	3 (9%)	3 (5%)	3 (10%)
Carcinoma	2 (8%)	5 (15%)	17 (27%)	7 (23%)
Adenocarcinoma				
Mammary			3 (5%)[d]	1 (3%)
Lung		1 (3%)	7 (11%)	5 (17%)
Other	1 (4%)	3 (9%)	6 (10%)	1 (3%)
Hepatocellular			1 (2%)	
Basaloid		1 (3%)		
Squamous	1 (4%)			
Other tumors	2 (8%)	4 (12%)	4 (6%)	1 (3%)
Neuroendocrine tumor			1 (2%)	1 (3%)
Leukemia			1 (2%)	
Baso-squamous tumor		1 (3%)		
Histiocytic sarcoma	2 (8%)	1 (3%)		
Myeloma		1 (3%)		
Granuloma		1 (3%)		
Hemangioma			2 (3%)	
Tumor totals	25	34	63	30

[a]One of 8.
[b]Five of 11.
[c]Four of 10 osteosarcomas had metastasis.
[d]Two of 3 mammary adenocarcinomas had metastasis.

Table 2. Tumor spectrum in *Trp53*$^{R172H/R172H}$, *Trp53*$^{R245W/R245W}$, and *Trp53*$^{R270H/R270H}$ mice.

	Genotype			
Tumor type	***Trp53*$^{-/-}$ (*N* = 18)**	***Trp53*$^{R172H/R172H}$ (*N* = 21)**	***Trp53*$^{R245W/R245W}$ (*N* = 89)**	***Trp53*$^{R270H/R270H}$ (*N* = 29)**
Lymphoma	15 (83%)	13 (62%)	67 (57%)	17 (59%)
Sarcoma	3 (17%)	7 (33%)	42 (36%)	8 (28%)
Osteosarcoma			4 (3%)[a]	2 (7%)[c]
Angiosarcoma	3 (17%)	4 (19%)	10 (9%)	1 (3%)
Spindle cell sarcoma		2 (10%)	4 (3%)	1 (3%)
Rhabdomyosarcoma				1 (3%)
Fibrosarcoma				1 (3%)
Hemangiosarcoma			6 (5%)	
Synovial sarcoma			1 (1%)	
Sarcoma, NOS		1 (5%)	17 (15%)	2 (7%)
Carcinoma		1 (5%)	2 (2%)	2 (7%)
Adenocarcinoma				1 (3%)
Other carcinoma		1 (5%)	2 (2%)[b]	1 (3%)
Other tumors			6 (5%)	2 (7%)
Glioblastoma multiforme			1 (1%)	
Leukemia			2 (2%)	
Neuroblastoma			1 (1%)	
Teratoma			1 (1%)	
Malignant peripheral nerve sheath tumor				1 (3%)
Melanoma			1 (1%)	1 (3%)
Tumor totals	18	21	117	29

[a]One of 4 osteosarcomas had metastasis.
[b]One of 2 carcinomas had metastasis.
[c]One of 2 osteosarcomas had metastasis.

mice also developed osteosarcoma, and one mouse from each genotype even had osteosarcoma metastasis (**Table 2**), which was not observed in *Trp53*$^{R172H/R172H}$ mice, indicating a distinct role of p53R245W and p53R270H in osteosarcomagenesis. Of note, more tumor types were observed in *Trp53*$^{R245W/R245W}$ and *Trp53*$^{R270H/R270H}$ mice, including glioblastoma multiforme, malignant peripheral nerve sheath tumor, and melanoma (**Table 2**), indicating tumor differences among homozygous mutant mice. Further, the average percentage of p53-positive nuclei (as measured by IHC) among all tumors from heterozygous and homozygous mutant mice was similar (**Fig. 3E**). To determine if the presence of p53 protein affected overall survival, tumors from *Trp53*$^{R245W/R245W}$ and *Trp53*$^{R270H/R270H}$ homozygous mice were categorized into two groups: one group with 0% to 40% p53-positive nuclei, and another group with 60% to 100% p53-positive nuclei (Supplementary Fig. S2A). Strikingly, the overall survival of mice with a higher percentage of p53-positive nuclei in tumors was significantly shorter (median survival at 132 days vs. 205 days; $P = 0.0059$; **Fig. 3F**), indicating that detection of p53R245W and p53R270H in tumor cells accelerates tumorigenesis in homozygous mice, thereby supporting GOF contributions to disease progression.

p53 mutant–specific differences in tumorigenesis and metastasis

Emerging evidence shows that different p53 mutants may have distinct GOF activities (11, 21). To examine allele-specific difference in tumorigenesis, lymphoma-specific survival was first assessed. Lymphomas were prominent in *Trp53*$^{R172H/+}$ and *Trp53*$^{R245W/+}$ mice, yet very few *Trp53*$^{R270H/+}$ mice had lymphoma as the only cancer, which is consistent with a previous study reporting that *Trp53*$^{R270H/+}$ in a $129S_4$/SvJae genetic background showed high incidence of carcinomas and multiple tumors per mouse (15). Therefore, the lymphoma-specific survival of *Trp53*$^{R245W/+}$ mice was compared with that of the *Trp53*$^{R172H/+}$ mice. *Trp53*$^{R245W/+}$ mice with only lymphoma (median survival, 421 days) died significantly faster than *Trp53*$^{R172H/+}$ mice (median survival, 518 days; $P = 0.0298$; **Fig. 4A**), suggesting p53R245W was more potent in driving lymphoma-specific lethality than p53R172H.

We also examined survival differences in mice with osteosarcoma as it is the second most common tumor type in *Trp53*$^{Mut/+}$ mice, notably, osteosarcomas occur with a higher frequency in female than male heterozygous mice (6 females vs. 2 males for *Trp53*$^{R172H/+}$ osteosarcomas, 8 females vs. 3 males for *Trp53*$^{R245W/+}$ osteosarcomas, and 10 females for *Trp53*$^{R270H/+}$ osteosarcomas), so we chose to restrict the downstream analysis to just female mice. Intriguingly, the overall survival of *Trp53*$^{R270H/+}$ female mice (median survival at 417 days) was significantly shorter than that of *Trp53*$^{R172H/+}$ female mice (median survival at 456 days; $P = 0.046$; **Fig. 4B**; Supplementary Fig. S2B), indicating that the p53R270H mutation is more tumorigenic than p53R172H in female mice. As all osteosarcomas lost the WT *Trp53* allele (determined in **Fig. 3C**), we were able to examine mutant p53 levels by IHC. The number of nuclei with detectable p53-mutant levels was similar among osteosarcomas from *Trp53*$^{R172H/+}$, *Trp53*$^{R245W/+}$, and *Trp53*$^{R270H/+}$ mice (**Fig. 4C**). However, the number of mice with metastasis was clearly higher in *Trp53*$^{R245W/+}$ (5/11, 45%) and *Trp53*$^{R270H/+}$ (4/10, 40%) mice than in *Trp53*$^{R172H/+}$ (1/8, 12.5%) mice (**Fig. 4D**; **Table 1**), indicating p53R245W and p53R270H-mutant proteins had stronger GOF contributing to osteosarcoma metastasis than p53R172H. The data combined from analyses of lymphomas and osteosarcomas indicated allele-specific differences in mice with different *p53* missense mutations.

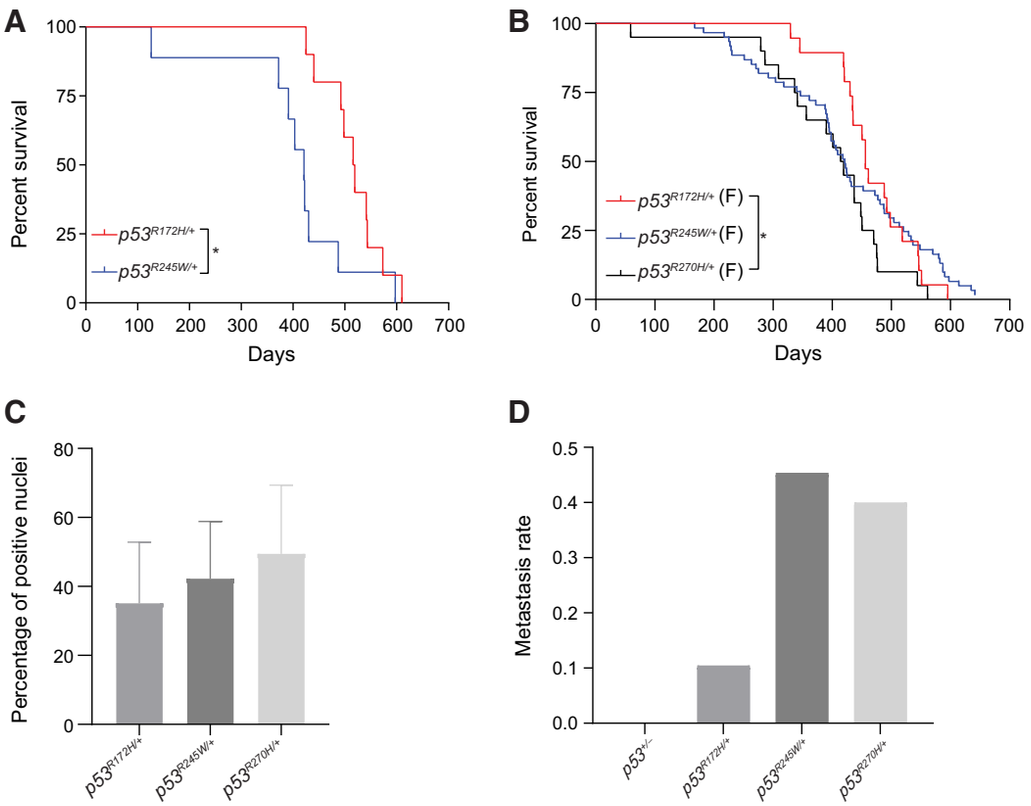

Figure 4.

Mutant allele-specific differences in tumorigenesis. **A,** Lymphoma-specific survival curves of $Trp53^{R172H/+}$ ($N = 10$) and $Trp53^{R245W/+}$ ($N = 9$) mice (lymphomas as the only cancer were not observed in $Trp53^{R270H/+}$). **B,** Female mouse-specific survival curves for the $Trp53^{R172H/+}$ ($N = 19$), $Trp53^{R245W/+}$ ($N = 60$), and $Trp53^{R270H/+}$ ($N = 20$) mice. **C,** p53 IHC staining in $Trp53^{R172H/+}$, $Trp53^{R245W/+}$, and $Trp53^{R270H/+}$ osteosarcomas. **D,** Percent metastasis observed in $Trp53^{+/-}$ (0/6), $Trp53^{R172H/+}$ (1/8), $Trp53^{R245W/+}$ (5/11), and $Trp53^{R270H/+}$ (4/10) mice. *, $P < 0.05$ by the t test.

The transcriptome of mutant p53-specific osteosarcomas supports allele-specific differences in GOF

The presence of osteosarcoma is a defining feature in LFS patients, and osteosarcomas develop more frequently than any other sarcomas in $Trp53^{Mut/+}$mice, with more metastasis in $Trp53^{R245W/+}$ and $Trp53^{R270H/+}$ mice than in $Trp53^{R172H/+}$ and $Trp53^{+/-}$ mice. These mouse models provided a platform to examine mutant-specific differences in a single tumor type. One mechanism of mutant p53 GOF is mediated by the interaction with other transcription factors to upregulate tumor-promoting pathways (13). Therefore, RNA-seq analysis was performed to identify mutant p53-driven transcriptomes of primary osteosarcoma tumor samples from $Trp53^{+/-}$ ($n = 4$), $Trp53^{R172H/+}$ ($n = 6$), $Trp53^{R245W/+}$ ($n = 3$), and $Trp53^{R270H/+}$ ($n = 5$) mice. DEGs were identified in $Trp53^{R172H/+}$, $Trp53^{R245W/+}$, and $Trp53^{R270H/+}$ tumors compared with $Trp53^{+/-}$ tumors by significance criteria of adjusted $P < 0.05$ and fold change > 2. We identified 88 DEGs for $Trp53^{R172H/+}$, 115 DEGs for $Trp53^{R245W/+}$, and 180 DEGs for $Trp53^{R270H/+}$ osteosarcomas (Supplementary Fig. S3A). The majority of DEGs from $Trp53^{R172H/+}$ (62/88; 70%), $Trp53^{R245W/+}$ (89/115; 77%) and $Trp53^{R270H/+}$ (164/180; 91%) osteosarcomas were nonoverlapping (Supplementary Fig. S3B). In addition, distinct individual clusters of DEGs among mutant p53 groups were discernible when compared with the heterozygous p53 group by supervised clustering based on genotype (**Fig. 5A**). Principal component analysis revealed that osteosarcomas from contact mutations $Trp53^{R245W/+}$ and $Trp53^{R270H/+}$ were separated from osteosarcomas from $Trp53^{+/-}$ and $Trp53^{R172H/+}$ (**Fig. 5B**). IPA was performed with these three groups of DEGs to identify dysregulated pathways that could potentially contribute to tumorigenesis and metastasis. Again, very few overlapping pathways were observed among these groups (Supplementary Table S3). These data suggest that different p53-mutants drive distinct transcriptomes that may contribute to osteosarcoma progression.

As mutant p53 proteins interact with other transcription factors to upregulate genes to promote tumorigenesis and metastasis, a Venn diagram was generated using only upregulated DEGs (**Fig. 5C**). No common DEGs was found among the three different mutants, further suggesting distinct mechanisms drive GOF in these different p53-mutant mice. To identify transcription factors that might account for these differences, a promoter analysis was performed using three tools (Enrichr, oPOSSUM, and IPA). Due to the differences in the algorithms deployed by these programs, we selected common transcription factors identified from all 3 programs as the strongest probability of binding mutant p53. Using this method, we identified 4 potential cofactors for $Trp53^{R172H/+}$ and 8 potential transcriptional cofactors each for $Trp53^{R245W/+}$ and $Trp53^{R270H/+}$ tumors (**Table 3**; Supplementary Table S4). Stat3 was identified to interact with both contact mutants, p53R245W and p53R270H, consistent with recent

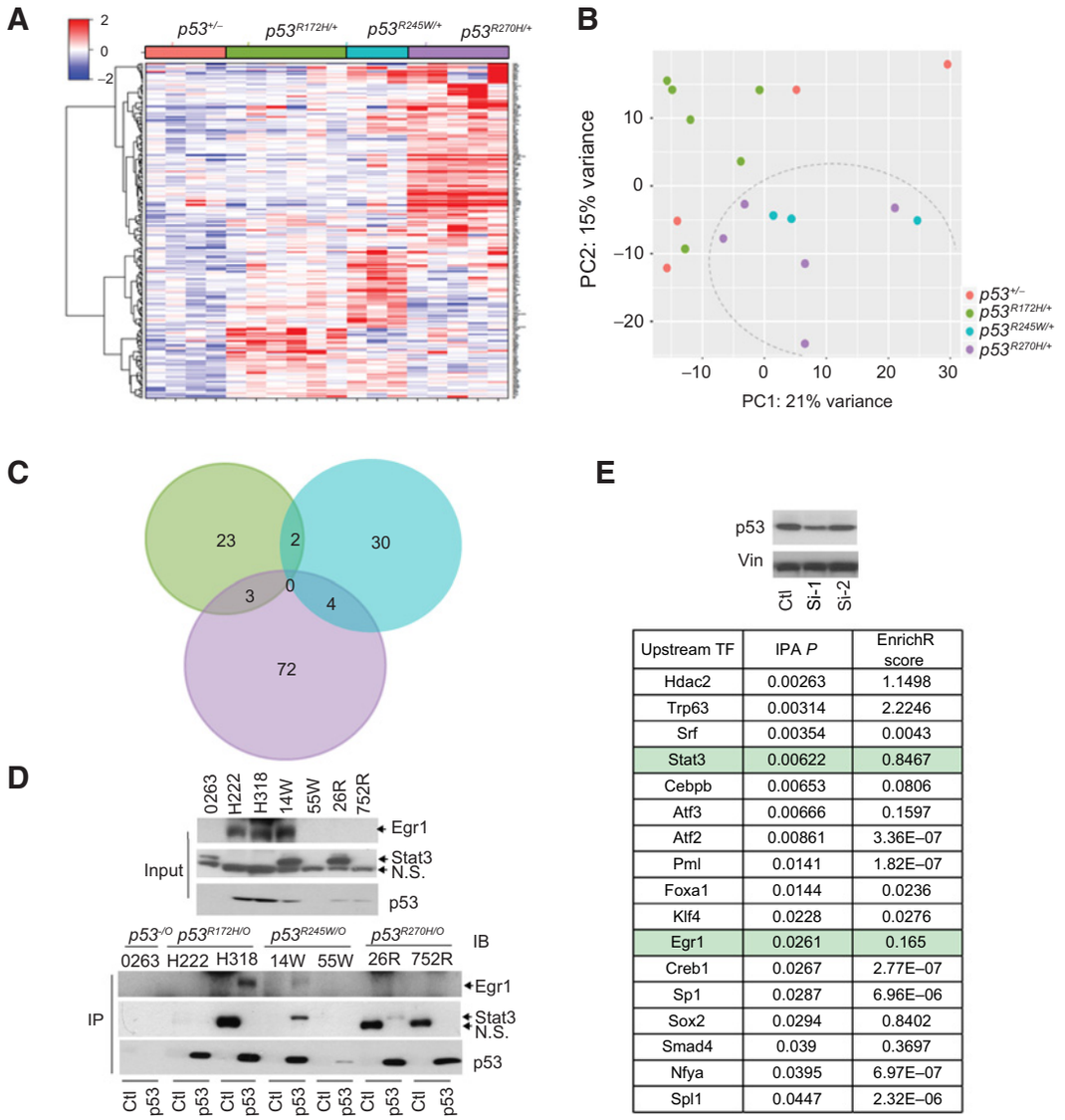

Upstream TF	IPA *P*	EnrichR score
Hdac2	0.00263	1.1498
Trp63	0.00314	2.2246
Srf	0.00354	0.0043
Stat3	0.00622	0.8467
Cebpb	0.00653	0.0806
Atf3	0.00666	0.1597
Atf2	0.00861	3.36E−07
Pml	0.0141	1.82E−07
Foxa1	0.0144	0.0236
Klf4	0.0228	0.0276
Egr1	0.0261	0.165
Creb1	0.0267	2.77E−07
Sp1	0.0287	6.96E−06
Sox2	0.0294	0.8402
Smad4	0.039	0.3697
Nfya	0.0395	6.97E−07
Spl1	0.0447	2.32E−06

Figure 5.

Different pathways contribute to osteosarcoma metastasis among p53 mutants. **A,** Supervised clustering based on genotype using the Pearson distance and Ward linkage. **B,** Principal component analysis of all osteosarcoma RNA-seq data. **C,** Upregulated DEGs for each mutant were identified by DESeq2 through comparing the individual *Trp53*$^{Mut/+}$ tumors with *Trp53*$^{+/-}$ tumors. The significance criteria were adjusted $P < 0.05$ and fold change > 2. **D,** Immunoprecipitation experiments were performed in primary osteosarcoma cell lines with LOH of the p53 WT allele (designated as O). Top, input. Ctl, control antibody for IP; p53, CM5 antip53 antibody. N.S., nonspecific; IP, immunoprecipitation; IB, immunoblot. **E,** IPA and Enrichr analysis results of top upstream transcription factors regulating the promoters of genes differentially expressed in 14W *Trp53*Si-1 cells. Ctl, control siRNA; Si-1 and Si-2, *Trp53*siRNA.

findings that human p53R248Q binds to Stat3, leading to GOF, in colorectal cancers (29). In addition, Yy1, which was previously shown to interact with WT p53 (30), was identified as a cofactor of p53R245W. Because p53R245W preserves protein structure similar to WT p53, it is not surprising to see Yy1 identified as a p53R245W binding protein. Thus, these data provide support for using this method to identify mutant p53 cotranscriptional factors. Novel factors were also identified as potential cotranscriptional factors for specific p53 mutants, including Klf4 and Ctcf for p53R172H; Ctcf, NFfe2l2, Tcf3, and Rest for p53R245W; and Myc, Runx1, Sp1, Max, and Srf for p53R270H (**Table 3**). Of note, the transcription factors Egr1 and Gata1 (also novel) were identified to be potentially associated with all three p53 mutants, indicating mutant p53 proteins also share some common interacting transcription factors (13).

To validate the cotranscriptional factors associated with mutant p53, immunoprecipitation experiments were performed using primary osteosarcoma cell lines from different *p53* germline mutations. Western blot analyses of 7 osteosarcoma cell lines showed three expressed Egr1 and three expressed Stat3, with one cell line expressing both proteins (**Fig. 5D**, top). Egr1 was immunoprecipitated with p53R172H in H318 cells and with p53R245W in 14W cells. Furthermore, Stat3 was immunoprecipitated with p53R245W in 14W cells

Table 3. Potential transcriptional cofactors associated with mutant p53 identified by overlapping Enrichr, oPOSSUM, and IPA analyses.

$p53^{R172H/+}$	$p53^{R245W/+}$	$p53^{R270H/+}$
Klf4	Ctcf	Myc
Egr1[a]	Nfe2l2	Gata1
Ctcf	Gata1	Runx1
Gata1[a]	Egr1	Egr1
	Stat3[b]	Sp1
	Tcf3	Stat3
	Rest	Max
	Yy1	Srf

[a]The common cofactors to all three mutants.
[b]Previously reported mutant p53 cofactor Stat3.

and with p53R270H in 26R cells (**Fig. 5D**, bottom). Clearly, the association of mutant p53 and cofactors was partially determined by the inherent expression of cofactors in the cell lines studied. In addition, although H222 cells have comparable expression levels of Egr1 to H318 and 14W cells, we did not observe association of p53R172H with Egr1, suggesting other factors also affect the interaction. As mutant p53 coimmunoprecipitated both Egr1 and Stat3 in 14W cells, we performed RNA-seq of 14W cells with and without *Trp53* siRNA knockdown to further examine whether mutant p53R245W upregulates target genes mediated by Egr1 and Stat3 (**Fig. 5E**). Many Egr1 and Stat3 target genes were downregulated in *Trp53* siRNA knockdown cells compared with scrambled controls (Supplementary Fig. S4). Moreover, using similar criteria to that used to perform promoter analyses of primary osteosarcomas, we identified predicted Egr1 and Stat3 binding sites upstream of the downmodulated promoters, validating the *in vitro* coimmunoprecipitation experiments (**Fig. 5E**).

Discussion

The generation of a germline $Trp53^{R245W}$ mouse model encompassing a major hotspot mutation in LFS patients allowed comparison of its activities with two other hotspot mutations $Trp53^{R172H}$ and $Trp53^{R270H}$ mice in a similar genetic background. Clearly, p53R245W is a loss-of-function mutation because homozygous $Trp53^{R245W/R245W}$ completely rescued the p53-dependent embryonic lethality of *Mdm2*-null mice. In addition, irradiated tissues from homozygous $Trp53^{R245W/R245W}$ mice showed no p53-dependent transcriptional activity of two p53 targets examined.

Mutant p53 proteins can inhibit WT p53 activity in cell lines. Because culture conditions affect p53 stability and activity, we provide the first comprehensive and side-by-side comparison of three p53 hotspot mutations *in vivo*. We examined the roles of IE for WT p53 and found that irradiated thymocytes from all three $Trp53^{Mut/+}$ mice showed similar IE. Similarly, in a compromised p53 background, all three $Trp53^{neo/Mut}$ mice showed similar survival that was significantly shorter than that of $Trp53^{neo/-}$ mice, indicating decreased WT p53 activity by mutant p53. These data, in particular, show that inhibition of WT p53 activity occurs *in vivo* and contributes to tumorigenesis.

Expression of the human hotspot p53 mutants p53R248W and p53R273H (the human equivalent of our p53R245W and p53R270H contact mutants) in MCF10A cells leads to increased invasion into the lumen in 3D culture than expression of p53R175H (the human equivalent of p53R172H; ref. 31). A somatic mouse mammary tumor model also demonstrated that the *Trp53R245W* mutation is more tumorigenic than *Trp53R172H* (21). These data indicate that these two contact mutants have a stronger GOF than the *Trp53R172H* structural mutation. Although $Trp53^{R270H/+}$ mice exhibit similar survival to $Trp53^{+/-}$ and $Trp53^{R172H/+}$ mice in a 129S/SvJae genetic background (15), our study showed that in a C57BL/6J background, $Trp53^{R245W/+}$ and $Trp53^{R270H/+}$ mice survive significantly less than $Trp53^{R172H/+}$ mice, providing additional support for p53 contact mutations (p53R245W and p53R270H) having a stronger GOF than the structural mutation p53R172H *in vivo*. Mouse background differences on tumor phenotypes in *Trp53* heterozygous mice have been previously observed (32). A detailed analysis of the GOF activities of osteosarcomas, a defining feature of LFS, was performed. Osteosarcomas from all $Trp53^{R172H/+}$, $Trp53^{R245W/+}$, and $Trp53^{R270H/+}$ mice studied lost the WT *Trp53* allele, indicating that in this tumor type, the presence of WT p53 prevented tumor development.

Our data further showed that while hotspot mutants retained a similar IE, they differed with regard to GOF with stronger activity in the two contact mutants studied. Mutant p53 proteins had distinct GOF mechanisms in driving tumorigenesis and metastasis *in vivo*. Furthermore, the IE was observed in irradiated thymocytes and in lymphomas of $Trp53^{neo/Mut}$ mice consistent with the previous observation that IE contributes significantly in myeloid malignancies (28). In contrast, GOF appears to be stronger in different tumor types such as osteosarcomas in our $Trp53^{Mut/+}$ mice (23, 25), in breast (31, 33–35), and in colorectal cancers (29). Thus, it is important to consider mutation and tumor types when evaluating IE or GOF of p53 missense mutations and in consideration of treatment options. Furthermore, our study identified multiple novel p53-associated cotranscriptional factors, such as Stat3 and Egr1, which might contribute to osteosarcoma metastasis. More investigation of these pathways may lead to new therapeutic strategies.

Authors' Disclosures

G. Lozano reports grants from NIH and grants from CPRIT during the conduct of the study. No disclosures were reported by the other authors.

Authors' Contributions

S. Xiong: Conceptualization, data curation, software, formal analysis, validation, investigation, visualization, methodology, writing–original draft. **D. Chachad:** Data curation, software, formal analysis, methodology, writing–original draft. **Y. Zhang:** Conceptualization, data curation, formal analysis. **J. Gencel-Augusto:** Data curation, investigation. **M. Sirito:** Data curation. **V. Pant:** Data curation. **P. Yang:** Resources. **C. Sun:** Data curation. **G. Chau:** Data curation. **Y. Qi:** Data curation, software. **X. Su:** Data curation, software. **E.M. Whitley:** Data curation. **A.K. El-Naggar:** Data curation. **G. Lozano:** Conceptualization, data curation, formal analysis, supervision, funding acquisition, methodology, writing–original draft, project administration, writing–review and editing.

Acknowledgments

The authors are grateful to the Genetically Engineered Mouse Facility and the Advanced Technology Genomics Core at MD Anderson Cancer Center (supported by the NIH/NCI through grant P30CA016672). They also thank Amando Guerra, Anushree Agrawal, and Nikita Williams for their technical support, and Amanda Wasylishen and Sydney Moyer for helpful discussion. The authors thank Sunita Patterson for editing this article. This work is supported by Cancer Prevention and Research Institute of Texas grant RP170231 and NIH grant CA82577 to G. Lozano and MD Anderson institutional research grant (2015-00051082-Y1) to S. Xiong.

The costs of publication of this article were defrayed in part by the payment of page charges. This article must therefore be hereby marked *advertisement* in accordance with 18 U.S.C. Section 1734 solely to indicate this fact.

Received October 5, 2021; revised February 3, 2022; accepted March 18, 2022; published first March 23, 2022.

References

1. Moyer SM, Wasylishen AR, Qi Y, Fowlkes N, Su X, Lozano G. p53 drives a transcriptional program that elicits a non-cell-autonomous response and alters cell state in vivo. Proc Natl Acad Sci U S A 2020;117:23663–73.
2. Eischen CM, Lozano G. The MDM network and its regulation of p53 activities: a rheostat of cancer risk. Hum Mutat 2014;35:728–37.
3. Liu Y, Tavana O, Gu W. p53 modifications: exquisite decorations of the powerful guardian. J Mol Cell Biol 2019;11:564–77.
4. Levine AJ. The many faces of p53: something for everyone. J Mol Cell Biol 2019; 11:524–30.
5. Patch AM, Christie EL, Etemadmoghadam D, Garsed DW, George J, Fereday S, et al. Whole-genome characterization of chemoresistant ovarian cancer. Nature 2015;521:489–94.
6. Bertheau P, Lehmann-Che J, Varna M, Dumay A, Poirot B, Porcher R, et al. p53 in breast cancer subtypes and new insights into response to chemotherapy. Breast 2013;22:S27–9.
7. Malkin D. Li-Fraumeni syndrome. Genes Cancer 2011;2:475–84.
8. Kansara M, Teng MW, Smyth MJ, Thomas DM. Translational biology of osteosarcoma. Nat Rev Cancer 2014;14:722–35.
9. Zhou X, Hao Q, Lu H. Mutant p53 in cancer therapy-the barrier or the path. J Mol Cell Biol 2019;11:293–305.
10. Mello SS, Attardi LD. Not all p53 gain-of-function mutants are created equal. Cell Death Differ 2013;20:855–7.
11. Hanel W, Marchenko N, Xu S, Yu SX, Weng W, Moll U. Two hot spot mutant p53 mouse models display differential gain of function in tumorigenesis. Cell Death Differ 2013;20:898–909.
12. Gencel-Augusto J, Lozano G. p53 tetramerization: at the center of the dominant-negative effect of mutant p53. Genes Dev 2020;34:1128–46.
13. Kim MP, Lozano G. Mutant p53 partners in crime. Cell Death Differ 2018;25: 161–8.
14. Lang GA, Iwakuma T, Suh YA, Liu G, Rao VA, Parant JM, et al. Gain of function of a p53 hot spot mutation in a mouse model of Li-Fraumeni syndrome. Cell 2004;119:861–72.
15. Olive KP, Tuveson DA, Ruhe ZC, Yin B, Willis NA, Bronson RT, et al. Mutant p53 gain of function in two mouse models of Li-Fraumeni syndrome. Cell 2004; 119:847–60.
16. Brosh R, Rotter V. When mutants gain new powers: news from the mutant p53 field. Nat Rev Cancer 2009;9:701–13.
17. Oren M, Rotter V. Mutant p53 gain-of-function in cancer. Cold Spring Harb Perspect Biol 2010;2:a001107.
18. Xu J, Qian J, Hu Y, Wang J, Zhou X, Chen H, et al. Heterogeneity of Li-Fraumeni syndrome links to unequal gain-of-function effects of p53 mutations. Sci Rep 2014;4:4223.
19. Donehower LA, Lozano G. 20 years studying p53 functions in genetically engineered mice. Nat Rev Cancer 2009;9:831–41.
20. Song H, Hollstein M, Xu Y. p53 gain-of-function cancer mutants induce genetic instability by inactivating ATM. Nat Cell Biol 2007;9:573–80.
21. Zhang Y, Xiong S, Liu B, Pant V, Celii F, Chau G, et al. Somatic Trp53 mutations differentially drive breast cancer and evolution of metastases. Nat Commun 2018;9:3953.
22. Wang Y, Suh YA, Fuller MY, Jackson JG, Xiong S, Terzian T, et al. Restoring expression of wild-type p53 suppresses tumor growth but does not cause tumor regression in mice with a p53 missense mutation. J Clin Invest 2011; 121:893–904.
23. Xiong S, Tu H, Kollareddy M, Pant V, Li Q, Zhang Y, et al. Pla2g16 phospholipase mediates gain-of-function activities of mutant p53. Proc Natl Acad Sci U S A 2014;111:11145–50.
24. Xiong S, Van Pelt CS, Elizondo-Fraire AC, Liu G, Lozano G. Synergistic roles of Mdm2 and Mdm4 for p53 inhibition in central nervous system development. Proc Natl Acad Sci U S A 2006;103:3226–31.
25. Pourebrahim R, Zhang Y, Liu B, Gao R, Xiong S, Lin PP, et al. Integrative genome analysis of somatic p53 mutant osteosarcomas identifies Ets2-dependent regulation of small nucleolar RNAs by mutant p53 protein. Genes Dev 2017;31: 1847–57.
26. Jones SN, Roe AE, Donehower LA, Bradley A. Rescue of embryonic lethality in Mdm2-deficient mice by absence of p53. Nature 1995;378:206–8.
27. Montes de Oca Luna R, Wagner DS, Lozano G. Rescue of early embryonic lethality in mdm2-deficient mice by deletion of p53. Nature 1995;378:203–6.
28. Boettcher S, Miller PG, Sharma R, McConkey M, Leventhal M, Krivtsov AV, et al. A dominant-negative effect drives selection of TP53 missense mutations in myeloid malignancies. Science 2019;365:599–604.
29. Schulz-Heddergott R, Stark N, Edmunds SJ, Li J, Conradi LC, Bohnenberger H, et al. Therapeutic Ablation of gain-of-function mutant p53 in colorectal cancer inhibits Stat3-mediated tumor growth and invasion. Cancer Cell 2018; 34:298–314.
30. Sui G, Affar el B, Shi Y, Brignone C, Wall NR, Yin P, et al. Yin Yang 1 is a negative regulator of p53. Cell 2004;117:859–72.
31. Freed-Pastor WA, Mizuno H, Zhao X, Langerod A, Moon SH, Rodriguez-Barrueco R, et al. Mutant p53 disrupts mammary tissue architecture via the mevalonate pathway. Cell 2012;148:244–58.
32. Koch JG, Gu X, Han Y, El-Naggar AK, Olson MV, Medina D, et al. Mammary tumor modifiers in BALB/cJ mice heterozygous for p53. Mamm Genome 2007; 18:300–9.
33. Adorno M, Cordenonsi M, Montagner M, Dupont S, Wong C, Hann B, et al. A mutant-p53/Smad complex opposes p63 to empower TGFbeta-induced metastasis. Cell 2009;137:87–98.
34. Do PM, Varanasi L, Fan S, Li C, Kubacka I, Newman V, et al. Mutant p53 cooperates with ETS2 to promote etoposide resistance. Genes Dev 2012;26: 830–45.
35. Stambolsky P, Tabach Y, Fontemaggi G, Weisz L, Maor-Aloni R, Siegfried Z, et al. Modulation of the vitamin D3 response by cancer-associated mutant p53. Cancer Cell 2010;17:273–85.